Marine Geophysical Research (2022) 43: 32
https://doi.org/10.1007/s11001-022-09494-w

ORIGINAL RESEARCH PAPER

Modeling of borehole washout effects and gas hydrate-filled fractures using NGHP-02 downhole data in Krishna Godavari offshore basin, India

Laxmi Pandey[1,2] · Maheswar Ojha[1,2]

Received: 4 March 2022 / Accepted: 23 July 2022 / Published online: 16 August 2022
© The Author(s), under exclusive licence to Springer Nature B.V. 2022

Abstract
The purpose of this study is to look into the effects of borehole washouts on log measurements and the resulting error in predicting gas hydrate saturation using well logs. We employ logging while drilling (LWD) data from the Indian National Gas Hydrate Program's second expedition (NGHP-02) in 2015. The NGHP-02 expedition discovered a significant amount of gas hydrate in coarse grain sediments in the Krishna Godavari (KG) Basin while drilling, coring, and logging. Borehole collapse or washout at particular depths in the presence of loose sediments impacted downhole log data at a few sites. We chose Holes NGHP-02-22A and NGHP-02-23A drilled in Area B of the KG Basin for our investigation and attempted to compensate washout effects in density-derived porosity, sonic and resistivity measurements, and the corresponding effects in estimating gas hydrate saturation. We use the sand-shale porosity model to remove the washout effects from density-derived porosity at washed-out depths. The corrected porosities and washout parameters are then used in rock physics theory to remove the washout effects from resistivity and velocity measurements by assuming washed-out zones as vertical fractures filled with seawater. We also estimate gas hydrate saturations from resistivity and velocity logs, taking into account both pore-filling and fracture-filling distributions. Analyzing velocity and resistivity logs jointly, we obtain fracture-filled porosity as 7.5% and 8% at Hole 02-22A and 02-23A respectively. Estimated saturation compared with that of the pressure core measurements show good correlation.

Keywords Borehole washout · Anisotropy · Fracture porosity · Gas hydrate saturation

Introduction

Gas hydrate, a naturally occurring compound of gas (primarily methane) and water, is recognised as a fuel of global interest due to its remarkable potential in reducing the energy crisis caused by fossil fuel scarcity. Gas hydrate is formed beneath permafrost and marine sediments under suitable low temperature and high pressure conditions (Kvenvolden 1988; Sloan and Koh 2007; Makogon 2010; Huang et al. 2020). Aside from the potential energy resource, methane hydrate dissociation can cause marine geohazards such as seafloor subsidence, slumps, and slides, as well as global climate change due to methane gas emissions into the atmosphere (Ruppel and Kessler 2017; Wang et al. 2020). Seismic and well log data are commonly used to detect the presence of gas hydrate in sediments. Using rock physics theories, the velocity and resistivity of the host sediments elevated in the presence of gas hydrate can be translated into the amount of gas hydrate (Ghosh et al. 2010; Wang et al. 2013; Phillips et al. 2014). Several studies have been conducted to characterise gas hydrate-bearing sediments in the KG Basin using well logs from the NGHP-01 and -02 expeditions (Jana et al. 2015, 2017; Ojha et al. 2016; Joshi et al. 2019; Pandey et al. 2019; Yadav et al. 2019; Singh et al. 2020; Ghosh and Ojha 2021). But, least attempts have been made in analyzing the effects of borehole washout and fracture porosity in estimating the gas hydrate saturation in this area.

In this study, we investigate the effect of borehole washouts on calculating gas hydrate saturation using velocity and resistivity logs at NGHP-02-22A and -02-23A of Area B in

✉ Maheswar Ojha
maheswar_ojha@ngri.res.in

[1] CSIR-National Geophysical Research Institute, Uppal Road, Hyderabad 500007, India

[2] Academy of Scientific and Innovative Research (AcSIR), Ghaziabad 201002, India

the KG Basin. We also try to obtain optimal fracture porosity by jointly analysing resistivity and sonic logs (Liu et al. 2020). Borehole washout, which is caused by the presence of loose and uncompacted sediments, can impact the measurements of numerous physical parameters during downhole logging. Because of the borehole fluid intrusion, the density measurement is the most affected log. We use sonic and resistivity logs to rectify the density-derived porosity, which is the most critical parameter for estimating gas hydrate saturations (Marion et al. 1992; Kolterman and Gorelick 1995; Lee 2012; Lee et al. 2012). Using resistivity and sonic logs, we analyse gas hydrate saturations at holes NGHP-02-22A and -02-23A in Area B of the KG Basin, considering the impacts of borehole washout as well as anisotropy due to fracture-filled gas hydrate. With and without addressing borehole washout effects, we notice considerable differences in gas hydrate saturation estimations. To ensure the accuracy of the findings, pressure core readings from Holes NGHP-02-22A and -02-23A were compared to the resistivity and velocity-derived gas hydrate saturations (pore-filling and fracture-filling).

Study area and data

The NGHP-01 expedition in 2006 found most of the gas hydrate deposits as fracture-fill in the clay-dominated sediments in the KG Basin (Collett et al. 2008). Whereas, the NGHP-02 expedition in 2015 conducted in deepwater of the KG Basin found gas hydrate deposits in the coarse-grained sand-bearing sediments at many sites (Collet et al. 2014; Boswell et al. 2019). The current study is carried out at Sites NGHP-02-22 and NGHP-02-23, located in Area-B of the KG Basin (Fig. 1).

Area B is characterized by a syncline present along the flanks of the regionally prominent anticlinal structure. The Site NGHP-02-22 is located off the main axis of the anticline at a water depth of 2557 m. At this well location, three holes were drilled, where the LWD data were acquired at Hole 02-22A, conventional coring was done at Hole 02-22B, and wireline logging (WLL), vertical seismic profiling (VSP), conventional and pressure coring were carried out at Hole 02-22C. The Site NGHP-02-23 is located along the crest of the anticline at a water depth of 2554 m.

LWD data were acquired at Hole 02-23A, conventional coring was done at Hole 02-23B, and WLL and pressure cores were collected at Hole 02-23-C (Waite et al. 2019). At NGHP-02-22, gas hydrate is distributed as fracture-filling at depths ranging from 100 to 190 mbsf, and as both pore- and fracture-filling at depths ranging from 207 to 290 mbsf, BSR depth (Collet et al. 2019; Ghosh and Ojha 2021). At Site NGHP-02-23, gas hydrate is distributed as fracture-filling at depths ranging from 165 to 198 mbsf and pore-filling at depths ranging

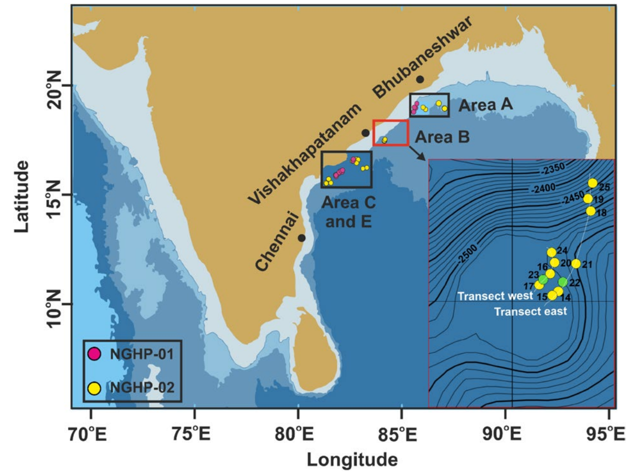

Fig. 1 Locations of the NGHP-01 (pink-filled circles) and -02 (yellow-filled circles) expedition sites in the KG and Mahanadi Basins. The zoomed section of the study area (red color rectangle) is shown as an inset, where Sites NGHP-02-22 and NGHP-02-23 are indicated by the green-filled circles

from 271 to 288 mbsf, BSR depth (Collett et al. 2019; Ghosh and Ojha 2021). The caliper, gamma-ray, bulk density, electrical resistivity, sonic velocity, and density-derived porosity used in this study at holes NGHP-02-22A and NGHP-02-23A are depicted in Fig. 2.

Methodology and results

First, we take into account the effects of significant borehole washouts and correct the density-derived porosity. Using this corrected porosity, we remove the washout effects from observed sonic and resistivity logs, and then calculate gas hydrate saturation for both pore- and fracture-filling distributions. For better understanding of the method used in this study, a flowchart is shown in Fig. 3. The details of the methods are briefly described below.

Borehole washout correction

The borehole washouts are indicated by large borehole diameters at various depths noticed from the caliper logs. We consider washed-out zones where the borehole diameter is larger than 9 inches for both holes (Fig. 2a, b). Diameter of the drill bit used in logging was 8.5 inches. The modified sand-shale porosity model (Kolterman and Gorelick 1995) of Marion et al. (1992) is used to rectify the influence of these washouts on density-derived porosity. The correction in porosity ($\Delta\phi$) is calculated as follows,

$$\Delta\phi = \phi_{sand} - y_1 V_{sh}\left(1 - \phi_{shale}\right) + \left(1 - y_1\right) V_{sh}\phi_{shale}, \text{ for } V_{sh} < \phi_{sand}, \quad (1)$$

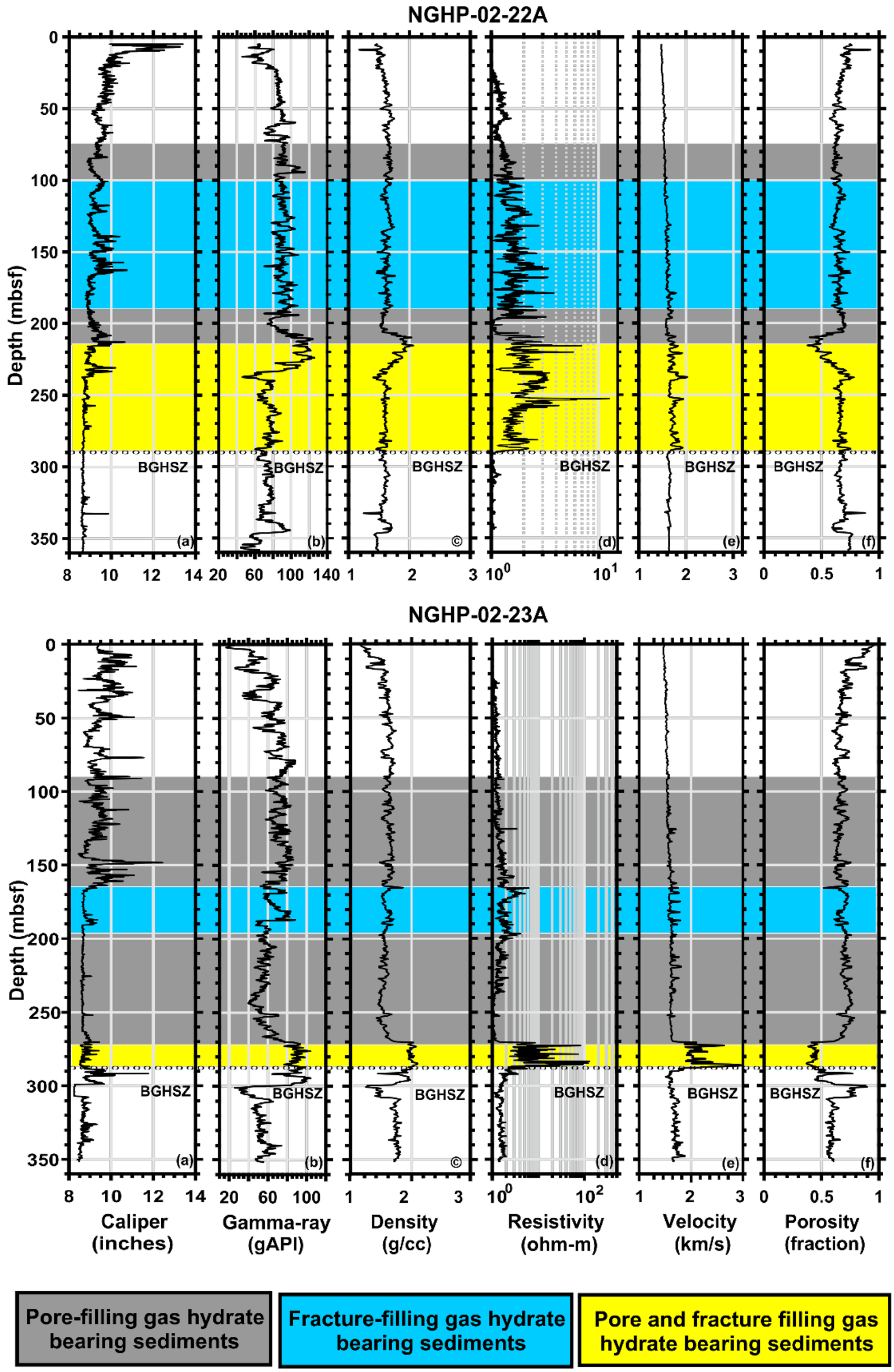

Fig. 2 LWD (a) caliper, (b) gamma-ray, (c) bulk density, (d) electrical resistivity, (e) sonic velocity logs and (f) density-derived porosity at Hole NGHP-02-22A (top panel) and NGHP-02-23A (bottom panel). The base of gas hydrate stability zone (BGHSZ) is marked by the dashed line

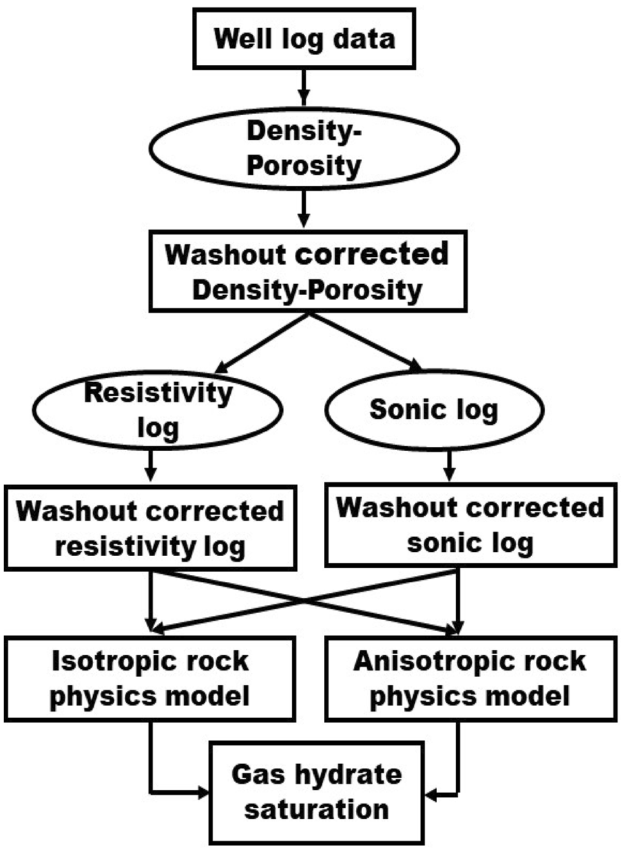

Fig. 3 Workflow of the methodology used in modeling of borehole washouts and fractures

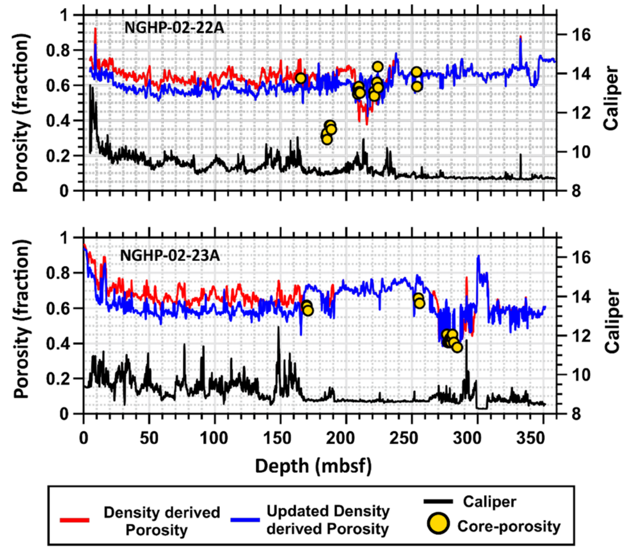

Fig. 4 Porosities derived from the density logs (red curves), the corrected density-porosities (blue curves) and core-derived porosity (yellow filled circles) at Hole NGHP-02-22A (top) and NGHP-02-23A (bottom). Caliper logs (black curves) with enlarged borehole diameter (inch) at various depths indicate the washout zones

and,

$$\Delta\phi = \phi_{shale}V_{sh} + \phi_{sand}\left(1 - y_2\right), \text{ for } V_{sh} \geq \phi_{sand}, \tag{2}$$

where $y_1 = V_{sh}(y_{min} - 1)/\phi_{sand} + 1$ and $y_2 = \left(V_{sh}-1\right)\left(1-y_{min}\right)/\left(1-\phi_{sand}\right) + 1$, ϕ_{sand} is the sand porosity,ϕ_{shale} is the shale porosity. For the marine sediments the value of y_{min} can be used as 0.78 (Pratson et al. 2003; Lee et al. 2012). V_{sh} is the shale volume computed using the gamma-ray log. ϕ_{sand} and ϕ_{shale} are used as 0.62 and 0.68 at Hole NGHP-02-22A and 0.60 and 0.65 at Hole NGHP-02-23A, respectively. The values of ϕ_{sand} and ϕ_{shale} are chosen from the corresponding depths of occurring sand and shale (clay) with no washout zones. Figure 4 shows the corrected density-derived porosities at Hole NGHP-02-22A and NGHP-02-23A. For the deriving porosity from density logs, the matrix density is used as 2.7 g/cm^3. Next, using this corrected-porosity, we correct sonic and resistivity logs.

Correction in resistivity log and estimation of pore-filling gas hydrate saturation

The resistivity of the fully water-saturated sediment (R_0) is calculated as,

$$R_0 = aR_w\phi^{-m}, \tag{3}$$

where a and m are Archie's constants obtained using the crossplot between the formation factor ($FF = R_O/R_w = a\phi^{-m}$) and density-derived porosity (ϕ). The constants, we obtain as a = 0.58, m = 3.5 at Hole NGHP-02-22A and a = 0.82, m = 3 for Hole NGHP-02-23A (Ghosh and Ojha 2021). The connate water resistivity R_w is computed using Arp's (1953) formula ($R_{w2} = R_{w1}(T_1 + 21.5)/(T_2 + 21.5)$), where, R_{w1} and R_{w2} are resistivity of water at the temperature T_1 (seafloor temperature) and T_2 (temperature at any depth below seafloor). Seafloor temperature is 3 °C. and the geothermal gradient is 64 °C/km at Hole 02-22A and 70 °C/km at Hole 02-23A. The resistivity of the fully water-saturated sediment (R_0) is corrected by considering the washed-out zone as a vertical fracture filled with seawater (Lee et al., 2012; Lee, 2012). R_0 in the washout zone is expressed (Kennedy and Herrick, 2004) as,

$$R_0 = (1 - V_{wash})[(\phi^m / aR_w) + ((1 - \phi)V_{sh}/R_c)] - 1 + V_{wash}R_{sw}, \quad (4)$$

with, $V_{wash} = \delta(1 - V_{sh})^3$ for $V_{sh} < V_{th}$

and $V_{wash} = 0$, for $V_{sh} =< V_{th}$,

where R_{sw} is the resistivity of seawater (0.4 Ω-m) and, R_C is the resistivity of clay (5 Ω-m). If $V_{wash} = 1$, the resistivity logging tool records the resistivity of seawater and if $V_{wash} = 0$, the tool records the true formation resistivity. The volume of washout, V_{wash} is proportionate to the sand volume present in the formation. The calibration factor δ is determined by matching the theoretical R_0 with observed resistivity at depths with no washout and no gas hydrate zones, which is obtained as 0.5 at Hole 02-22A and 0.55 at Hole 02-23A. V_{th} is the threshold volume fraction of shale, below which it indicates the uncompacted and above which it indicates the compacted sediments The threshold shale volume (V_{th}) is obtained from the gamma-ray log by observing a trend, which is 0.32 and 0.35 at Holes 02-22A and 02-23A, respectively. Figure 5 depicts a comparison of resistivities of fully water-saturated sediments without and with washout effects at Holes 02-22A and 02-23A. Difference between washout corrected R_0 (yellow curve in Fig. 5) and theoretical R_0 (blue curve in Fig. 5) is the correction to the measured formation resistivity (R_t). Using the corrected porosity and

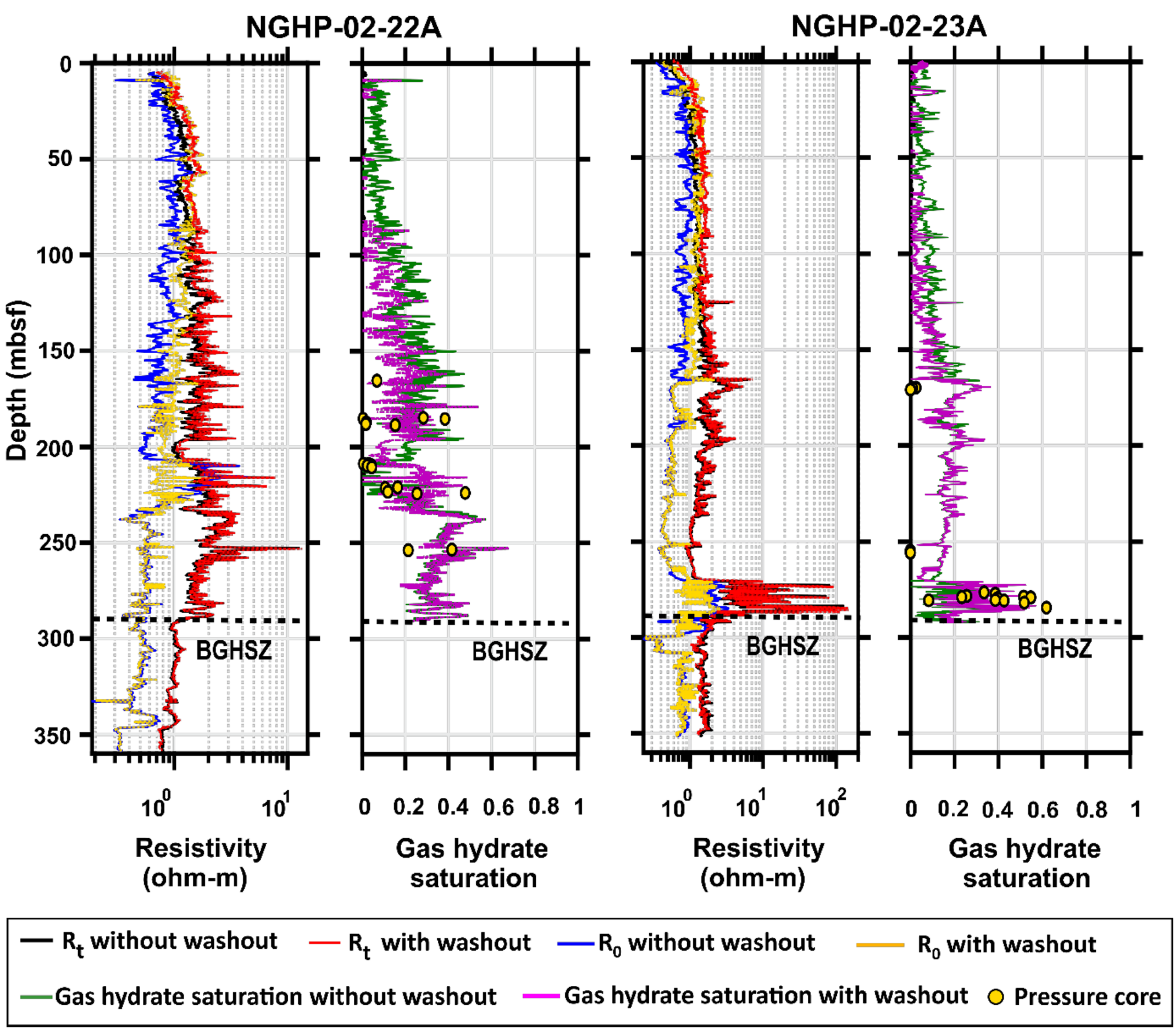

Fig. 5 Resistivity of fully water-saturated sediment (R_0) without (blue curves) and with (yellow), measured resistivities (R_t) without (black curves) and with (red curve) washout correction. Corresponding pore-filling gas hydrate saturation without (green) and with (purple) washout correction to the measured resistivity at Holes NGHP-02-22A and NGHP-02-23A. Black circles filled with yellow are gas hydrate saturation from pressure core measurements. Density-derived porosity used here is corrected for washout

corrected R_t, we calculate gas hydrate saturation for pore-filling distribution. The amount of water (S_w) present in the pores of the sediment is calculated (Archie 1942) as,

$$S_w = \left(\frac{R_0}{R_t}\right)^{\frac{1}{n}}, \quad (5)$$

where n is the saturation exponent. Amount of gas hydrate is calculated as,

$$S_h = 1 - S_w. \quad (6)$$

We can see a significant difference in saturation estimated without (green curve in Fig. 5) and with (purple curve in Fig. 5) considering the effects of washouts on measured resistivities, within the depth intervals 0–150 mbsf at Hole 02-22A and 0–70 mbsf at Hole 02-23A.

Correction in sonic log and estimation of pore-filling gas hydrate saturation

For a medium consisting of two components, any elastic parameter (G) can be calculated (White 1965) as,

$$\langle G \rangle \equiv \eta_1 G_1 + \eta_2 G_2, \quad (7)$$

$$\left\langle \frac{1}{G} \right\rangle^{-1} \equiv \left(\frac{\eta_1}{G_1} + \frac{\eta_2}{G_2}\right)^{-1}, \quad (8)$$

where η_1 and η_2 are the volume fraction of the first and second component respectively. For correcting sonic measurements due to washout, we assume a two-component medium, one component is seawater-filled vertical fracture and another component is the host sediment (Lee et al. 2012; Lee 2012). The P-wave velocity (V_P) is calculated using equations in terms of Lame's parameters λ and μ as,

$$V_P = (A/\rho)^{1/2}, \quad (9)$$

where $A = \langle \frac{4\mu(\lambda+\mu)}{\lambda+2\mu} \rangle + \langle \frac{1}{\lambda+2\mu} \rangle^{-1} \langle \frac{\lambda}{\lambda+2\mu} \rangle^{2}$, and $\rho = \langle \rho \rangle$,

If the first component is washed-out volume (V_{wash}), then $\eta_1 = V_{wash}$, which is expressed as, $V_{wash} = \delta(1 - V_{wash})^3$ for $V_{sh} < V_{th}$, $V_{wash} = 0$ for $V_{sh} =< V_{th}$.

Where δ is a calibration factor, which is determined by matching the theoretical V_P with observed V_P at no gas hydrate and no washed-out zone. We obtain δ as 0.88 at Hole 02-22A and 0.55 at 02-23A. If$V_{wash} = 1$, the sonic logging tool records the velocity of seawater and if$V_{wash} = 0$, the tool records the true formation velocity. The volume of washout, V_{wash} is proportionate to the sand volume present in the formation. Threshold shale volume (V_{th}) is used as 0.32 and 0.35 at Holes 02-22A and 02-23A, respectively. Parameters used to model the washed-out zones at Hole 02-22A are P-wave velocity $V_{P1} = 1.5$ km/s, S-wave velocity $V_{S1} = 0.001$ km/s, density $\rho_1 = 1.03$ g/cm^3, for the seawater-filled fracture and for the host sediment, $V_{P2} = 1.786$ km/s, $V_{S2} = 0.27$ km/s, and $\rho_2 = 1.52$ g/cm^3. While at Hole 02-23A, the parameters used are $V_{P1} = 1.5$ km/s, $V_{S1} = 0.001$ km/s, $\rho_1 = 1.03$ g/cm^3 for the seawater-filled fracture and for the host sediment, $V_{P2} = 1.713$ km/s, $V_{S2} = 0.21$ km/s, and $\rho_2 = 1.652$ g/cm^3. The parameter δ used in obtaining the washout volume (V_{wash}) is 0.88 at Hole 02-22A and 0.55 at Hole 02-23A. The volume of shale (V_{sh}) used is derived from the gamma-ray log. The threshold shale volume V_{th} is used as 0.32 and 0.35 at Hole 02-22A and 02-23A, respectively. Various elastic parameters used in velocity modeling are given in Table 1 (Appendix A). We use three-phase Biot-type equation (Lee and Collett 2009) for calculating velocity of the host sediment (2nd component). There are many theories available in the published literature that relate the elevated velocity of the sediments in terms of the amount of gas hydrate available in pores (Lee et al. 1996; Ecker et al. 1998; Dvorkin et al. 1999, 2003; Helgerud et al. 1999; Tinivella 1999; Jakobsen et al. 2000; Dai et al. 2008; Lee and Collett 2009; Ghosh et al. 2010). In this study, we use the three-phase Biot-type equation (TPBE), which is simple and provide satisfactory results in highly porous unconsolidated marine sediments (Sain and Ojha 2008; Ojha and Sain 2013; Lee and Collett 2009; Ojha and Ghosh 2021) without considering the anisotropy due to the orientation of clay platelets (Ghosh and Ojha 2021). Figure 6 shows the comparison of pore-filling gas hydrate saturation with and without considering borehole washouts in calculating water-saturated velocity at Holes 02-22A and 02-23A. We observe a substantial difference in the saturation estimated with and without considering borehole washout effects. After applying the washout corrections to sonic and resistivity logs measurements we use them to estimate fracture-filling gas hydrate saturation at two holes.

Fracture-filling gas hydrate saturation from velocity and resistivity logs

To estimate the amount of gas hydrate deposited as fracture-filling, at first, we should identify those fractures. For this, we analyse resistivity-at-bit (RAB) image, RING and propagation resistivity and sonic logs. From the RAB images (Fig. 7), it is noticed that the identified vertical to near-vertical resistive fractures are present in clay-dominated sediments at the depth intervals of ~108–290 mbsf at Hole 02-22A and from ~92–255 mbsf at Hole 02-23A.

The LWD propagation (phase and attenuation) resistivity logs (Fig. 8) acquired at Hole NGHP-02-22A and -02-23A confirm the presence of RAB image-inferred

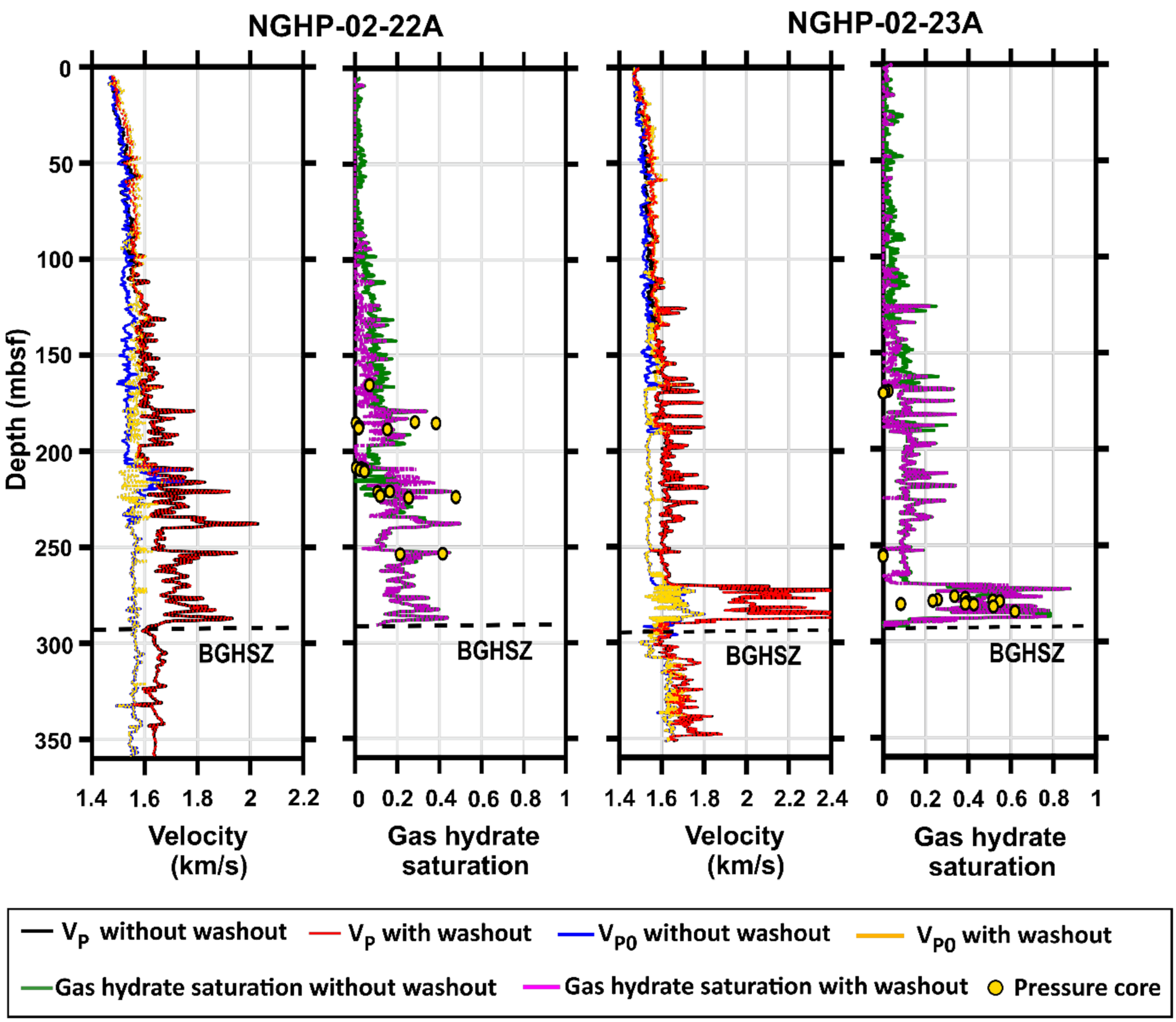

Fig. 6 Fully water-saturated theoretical sediment velocities (V_{P0}) without (blue curves) and with (dotted yellow) corrected porosity. Measured P-wave velocities (V_P) without (black curves) and with (dotted red) washout correction. Corresponding gas hydrate saturation without (green) and with (dotted purple) borehole washouts corrections to the observed velocities are shown at Holes NGHP-02-22A and NGHP-02-23A. Black circles filled with yellow are gas hydrate saturation from pressure core measurements

stratigraphic units with near vertical to vertical gas hydrate filled resistive fractures. Figure 8 shows the separation between the phase and attenuation resistivity curves, which are likely due to the occurrence of resistive gas hydrates in the fractures identified from image logs. These separations also illustrate that if resistive gas hydrates are present in the vertical fractures then the phase resistivity log (P40H or P16L) values exceed the attenuation resistivity (A40H and A16L) log values at the corresponding depths of high angle-gas hydrate filled fractures. Fractures identified from the RAB image logs (Fig. 7) and separations observed between the propagation resistivity curves (Fig. 8) assure the presence of fractures with dip 82º, 80º, 70º, 68º and 52º within the depth range of 167–256 mbsf at Hole 02-22A and 72º, 68º, 65º, 62º, 58º and 39º within the depth range of 106–240 mbsf at Hole 02-23A.

Next, we analyse the presence of fractures by crossplotting the formation factor (resistivity) and sonic log (Fig. 9). The trend of both formation factors and velocities (scaled) follows each other except at a few depth intervals, which are possibly due to the presence of near-vertical to vertical fractures (Lee and Collett, 2012).

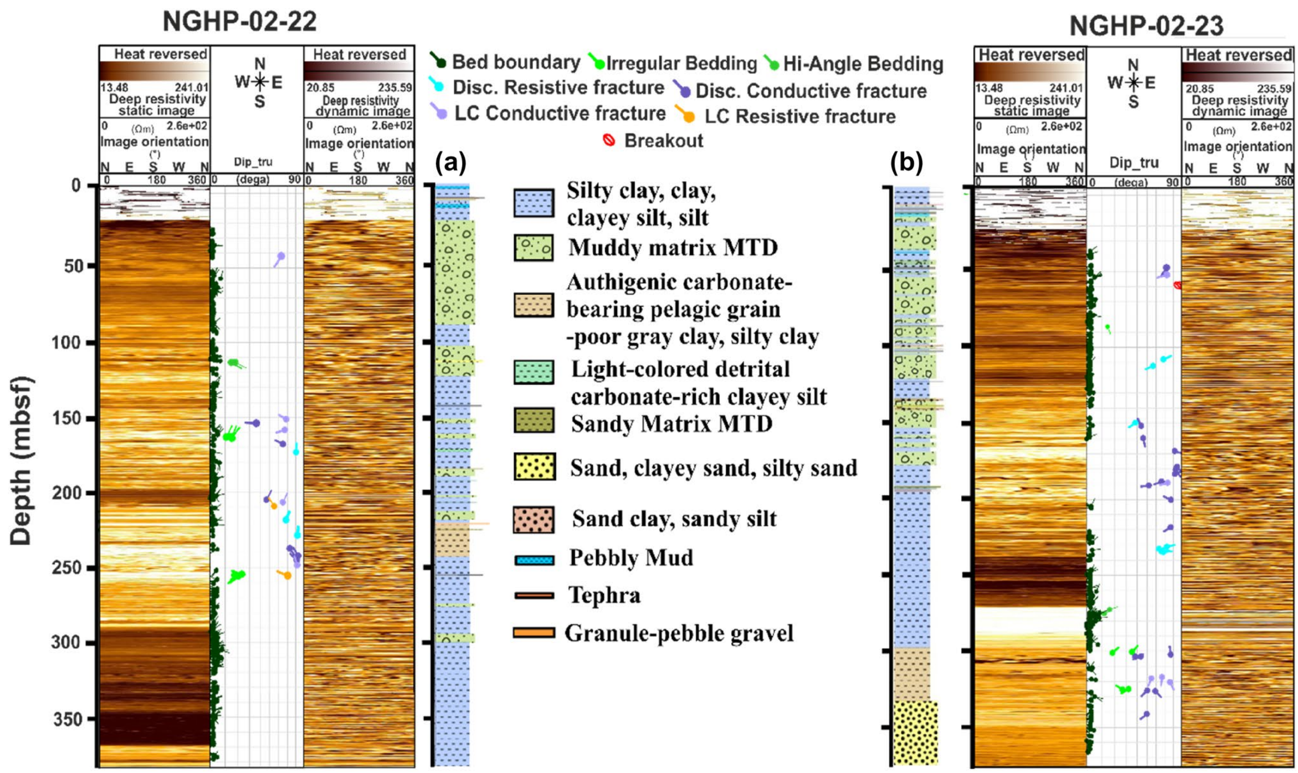

Fig. 7 A section of 360º unwrapped LWD GeoVISION resistivity-at-bit (RAB) image logs and core lithology at Hole NGHP-02-22A (left panel) and NGHP-02-23A (right panel). Disc and LC are the short form of discontinuous and low confidence, respectively

After analysing the presence of fractures qualitatively, it is important to know the amount of fractures present in sediments. Using only sonic or resistivity logs, it is very difficult to quantify the fractures. For this, we crossplot formation factors and velocities at two holes (Fig. 10), where red dots represent whole data and green dots represent the mismatched data in Fig. 9. Theoretical curves are computed for both pore-filling, and fracture-filling gas hydrate with dips 0º and 90º and fracture porosity of 7.5, 7 and 5% at Hole 02-22A and 8, 6 and 4% at Hole 02-23A. From Fig. 10, it is observed that the vertical fractures with fracture porosity of 7.5% at Hole 02-22A and 8% at Hole 02-23A are matching well with mismatched data. Using these fracture porosity, we show theoretical responses for different dip angles of fractures at Holes 02-22A and 02-23A in Fig. 11. The presence of gas hydrate-filled fractures in mismatched zones (Fig. 9) is well correlated with the fractures identified from the RAB images (Fig. 7). The details of the theory for calculating the velocity of gas hydrate-filled fractures (Lee and Collett, 2009) are given in Appendix A. In Figs. 10 and 11, the water-filled porosities of 55% at Hole 02-22A and 63% at Hole 02-23A are chosen from the corrected density-derived porosity of the respective sites. The model parameters used for the fractures filled with 100% gas hydrate are V_{P1}=3.744 km/s, V_{S1} =1.946 km/s, and ρ_1=0.926 g/cm^3. The velocities for the isotropic medium composed of water-saturated sediments (end-member case 2) are modeled using the three-phase Biot type equation with the parameters given in Table 1 (Appendix A) at Holes 02-22A and 02-23A. For modelling of fracture-filling (anisotropic) gas hydrate using resistivity logs, we consider a medium composed of two components, in which component 1 is fracture filled with 100% gas hydrate (volume fraction of η and fracture porosity ϕ_1) and component 2 is fully water-saturated sediments with the porosity ϕ_2 and volume fraction $(1-\eta)$. In a fractured medium, there are two formation factors (Kennedy and Herrick 2004), one parallel to the fracture (F_h) and another perpendicular to the fracture (F_v), which are expressed as,

$$F_h = \frac{1}{\frac{\eta\phi_1^{m1}}{\alpha 1} + \frac{(1-\eta)\phi_2^{m2}}{\alpha 2}} \text{and} F_v = \frac{\frac{\eta\phi_1^{m1}}{\alpha 1} + \frac{(1-\eta)\phi_2^{m2}}{\alpha 2}}{\frac{\phi_1^{m1}\phi_2^{m2}}{(\alpha 1\alpha 2)}},$$

where the effective anisotropic formation factor is written as,

$$F_{xx} = F_h\cos^2\theta + F_v\sin^2\theta, \tag{10}$$

where θ is the fracture angle. Parameters used to model the second component (fully water-saturated sediment) are the

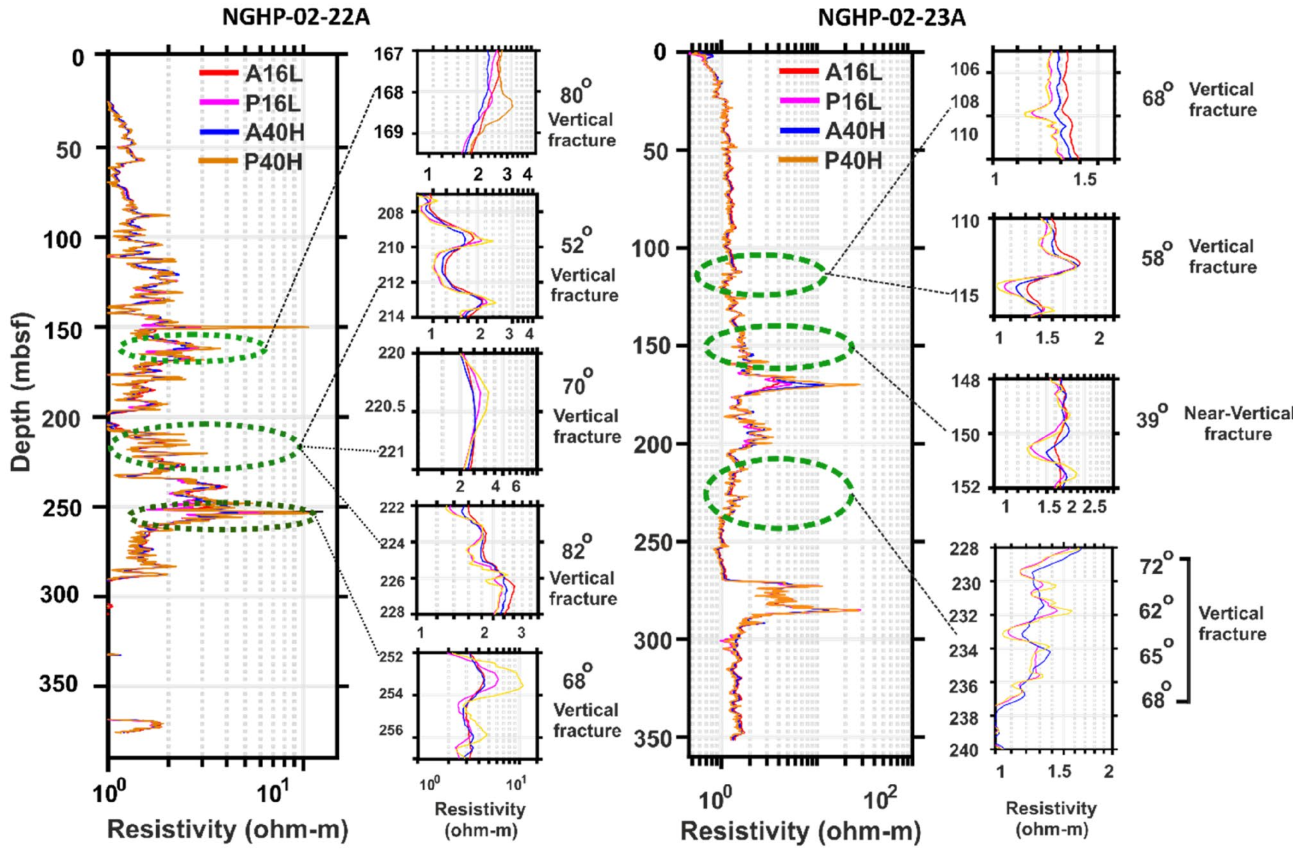

Fig. 8 LWD RING resistivity and propagation resistivity (phase and attenuation) measured at low (400 kHz) and high (2 MHz) frequencies at a source-receiver spacing of 16 and 40 inches at Hole NGHP-02-22A and NGHP-02-23A. Gas hydrate-filled vertical fractures (with dip 39°, 52°, 58°, 62°, 65°, 68°, 70°, 72°, 80°, 82°) identified from RAB images are encircled in green and depict the separation between the propagation resistivity curve at different depths

same as those used for isotropic resistivity modeling. The formation factor of component 2 (water-bearing sediments) can be computed using the recorded resistivity measurements and isotropic Archie's empirical equation. In case of fracture, the formation factor is a function of a representative porosity ϕ_1, which is not the true porosity of the fracture.

Next, the isotropic and anisotropic modeled responses of resistivity and velocity are translated into corresponding gas hydrate saturation. Figure 12 shows the comparison of velocity-derived saturations with the pressure core observations at Hole 02-22A and 02-23A. Figure 13 shows the comparison of resistivity-derived saturation estimates with the pressure core observations at Hole 02-22A and 02-23A. It is observed from Figs. 12 and 13 that the gas hydrate saturation obtained using resistivity logs for both pore- and fracture-filling match well with the pressure core measurements. However, a substantial discrepancy can be observed between the velocity-derived saturation estimates and pressure-core measurements, which may be due to the lower resolution of velocity compared to that of resistivity.

Discussion

In this study, we look into the effects of washout on porosity, velocity, and resistivity measurements taken at the KG basin's Holes NGHP-02-22A and -02-23A. Washout effects in log measurements are mostly compensated for during well log data acquisition and processing. In this study, the sand-shale porosity (KG) model is used to correct the erroneous density-derived porosity log values. The effects of washout on velocity and resistivity log responses are compensated for in the study using a vertical fracture model, with the washout zone assumed to be a vertical fracture occupied by seawater. The washout effects on velocity logs are found to be more complicated and nonlinear than those on resistivity logs. It is critical for the

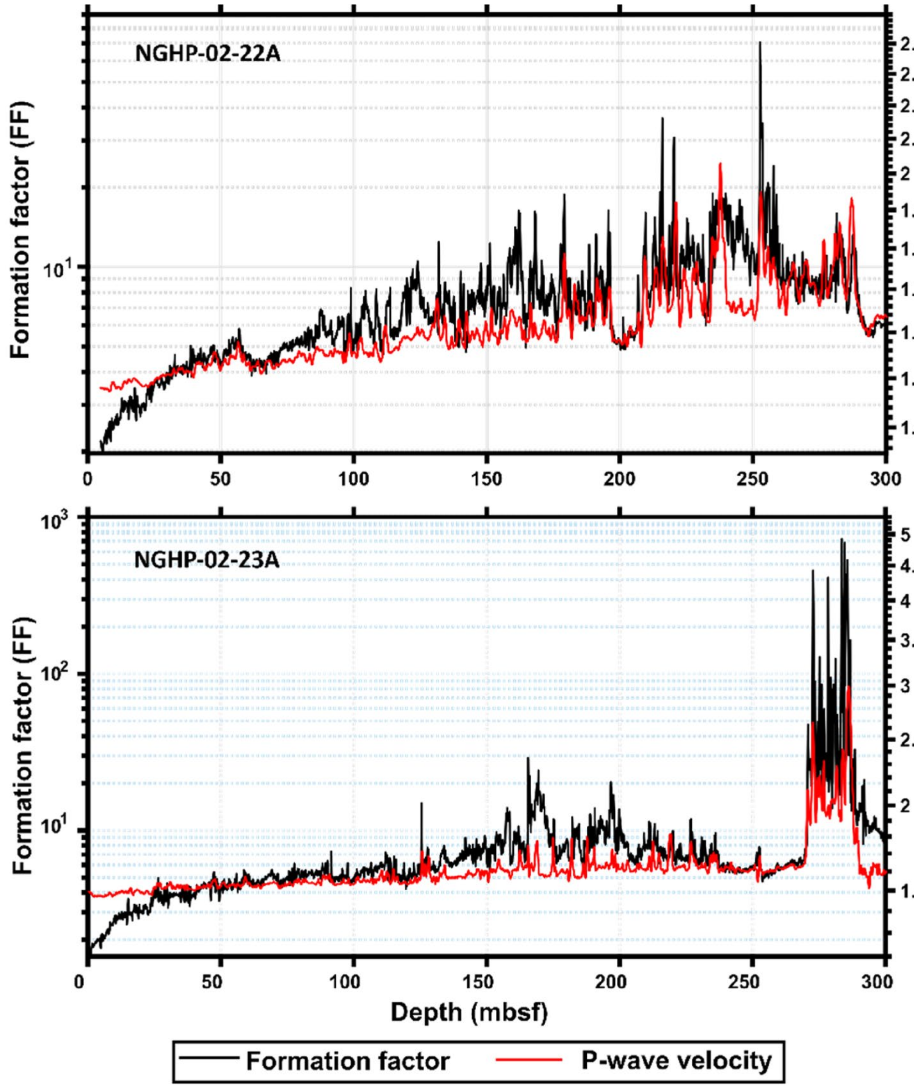

Fig. 9 Plots of formation factors and P-wave velocities at Hole NGHP-02-22A and NGHP-02-23A. Mismatched zones indicate the probable washout effects and presence of near-vertical to vertical fractures

quantitative analysis to accurately determine the size of the washout responsible for the degradations in the log measurements. The washout compensation model assumes that the size of the washout has a direct relationship with the sand volume and an inverse relationship with the shale volume. However, the preceding scenario is not valid if there is significant scattering in the volume of shale and caliper data. The presence of gas hydrates in washout columns is most likely due to uncertainties in Archie's parameters or to the effects of washouts at both sites. However, obtaining an exact amount of gas hydrate saturation value is difficult because there is a large difference between the saturation estimated by both the resistivity and velocity-based methods. Other possible explanations for this significant difference include the source-receiver spacing relative to the washout zone, which varies depending on the tool used in logging, as well as the effects of washout size, which varies from log to log.

The research also looks into the gas hydrate-filled fracture characteristics for different dip angles, as well as the corresponding gas hydrate saturation estimates. The estimated gas hydrate saturations at the respective sites are comparable to the pressure core-derived saturations. According to previous research, gas hydrate is most commonly found in clay-dominated sediments as near-vertical to vertical fractures (Collett et al. 2008; Cook and Goldberg 2008; Cook 2010; Lee and Collett 2012; Liu et al. 2020). The fracture porosity is a dominant and significant factor in estimating fracture dips and corresponding hydrate saturations (Lee and Collett 2012). During the modelling of the gas hydrate-filled fractured reservoir, we must choose the porosity of the fracture very precisely. However, utilising resistivity and velocity as independent quantities will not allow us to make this decision. So, in Hole 02-22A and 02-23A, we undertake a joint analysis of resistivity and velocity characteristics for various fracture dips to determine the correct fracture porosity of

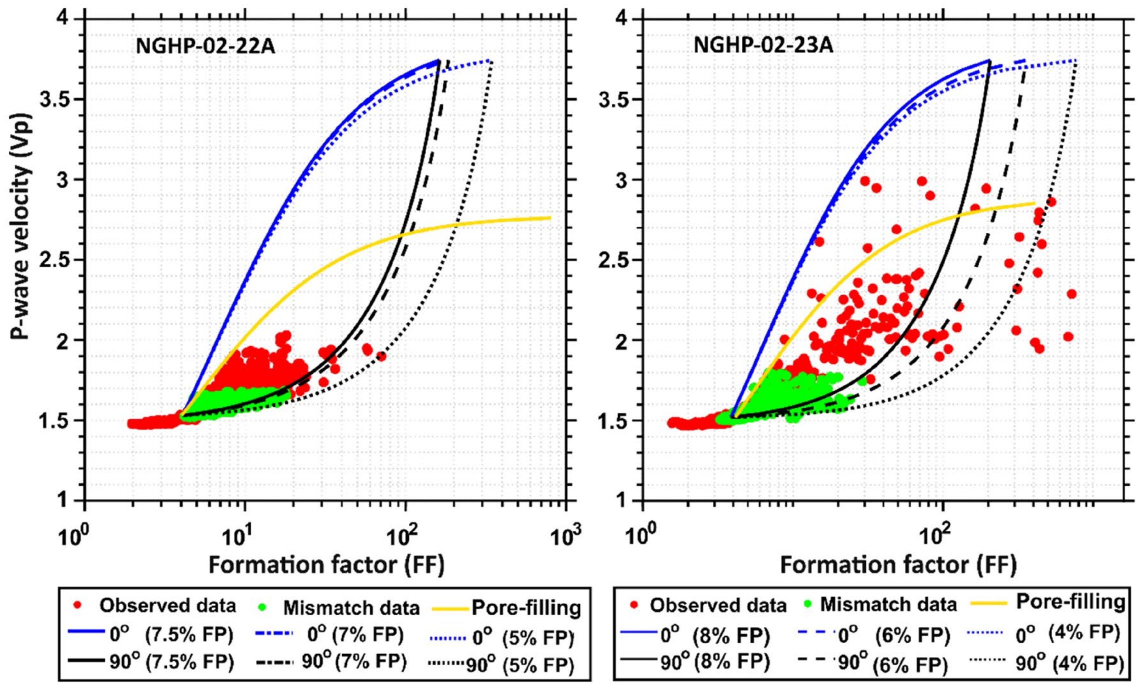

Fig. 10 Crossplot between anisotropic modelled responses of formation factor and P-wave velocity, assuming fracture porosity of 7.5, 7, 5% at Hole NGHP-02-22A and 8, 6, 4% at Hole NGHP-02-23A. Mismatch data refers to Fig. 9

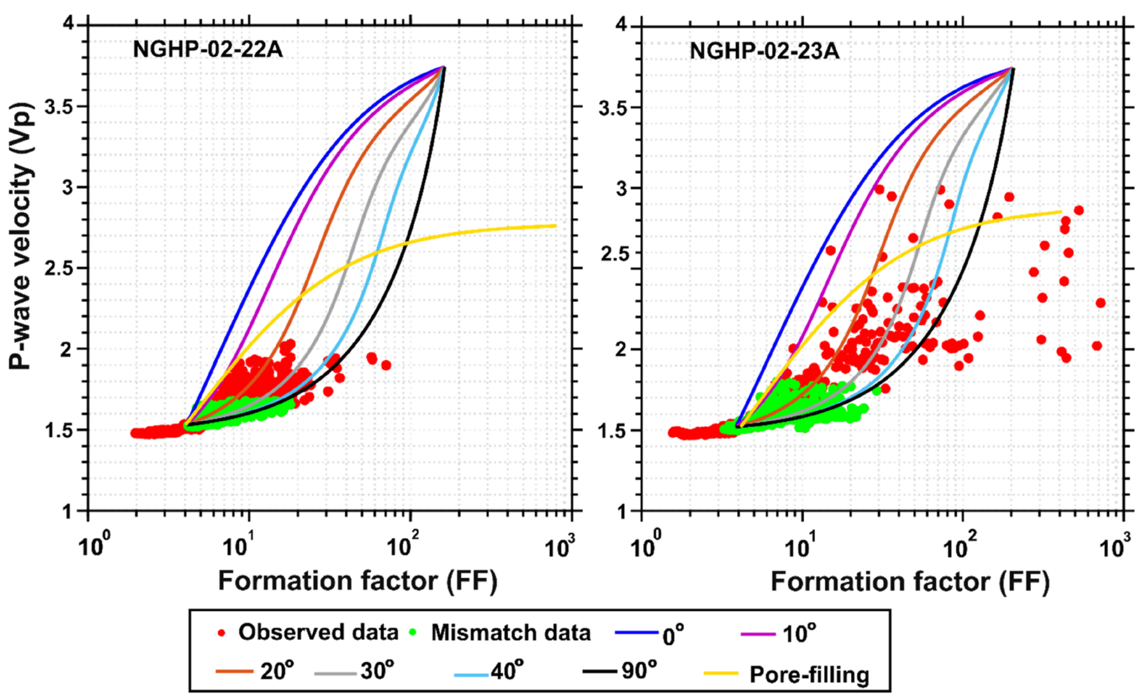

Fig. 11 Crossplot between anisotropic modelled responses of formation factor and P-wave velocity for various resistive fractures with a fracture porosity decided as 7.5% at Hole NGHP-02-22A and 8% at Hole NGHP-02-23A. Mismatch data refers to Fig. 9

7.5 and 8%. Fracture dips exceeding 40° are not included in the crossplot of anisotropic model responses of formation factor and velocity since they are found to respond similarly to vertical fractures. In the resistivity and velocity-based anisotropic numerical model, the volume fraction of fracture is assumed to be identical to the volume percent of gas hydrate.

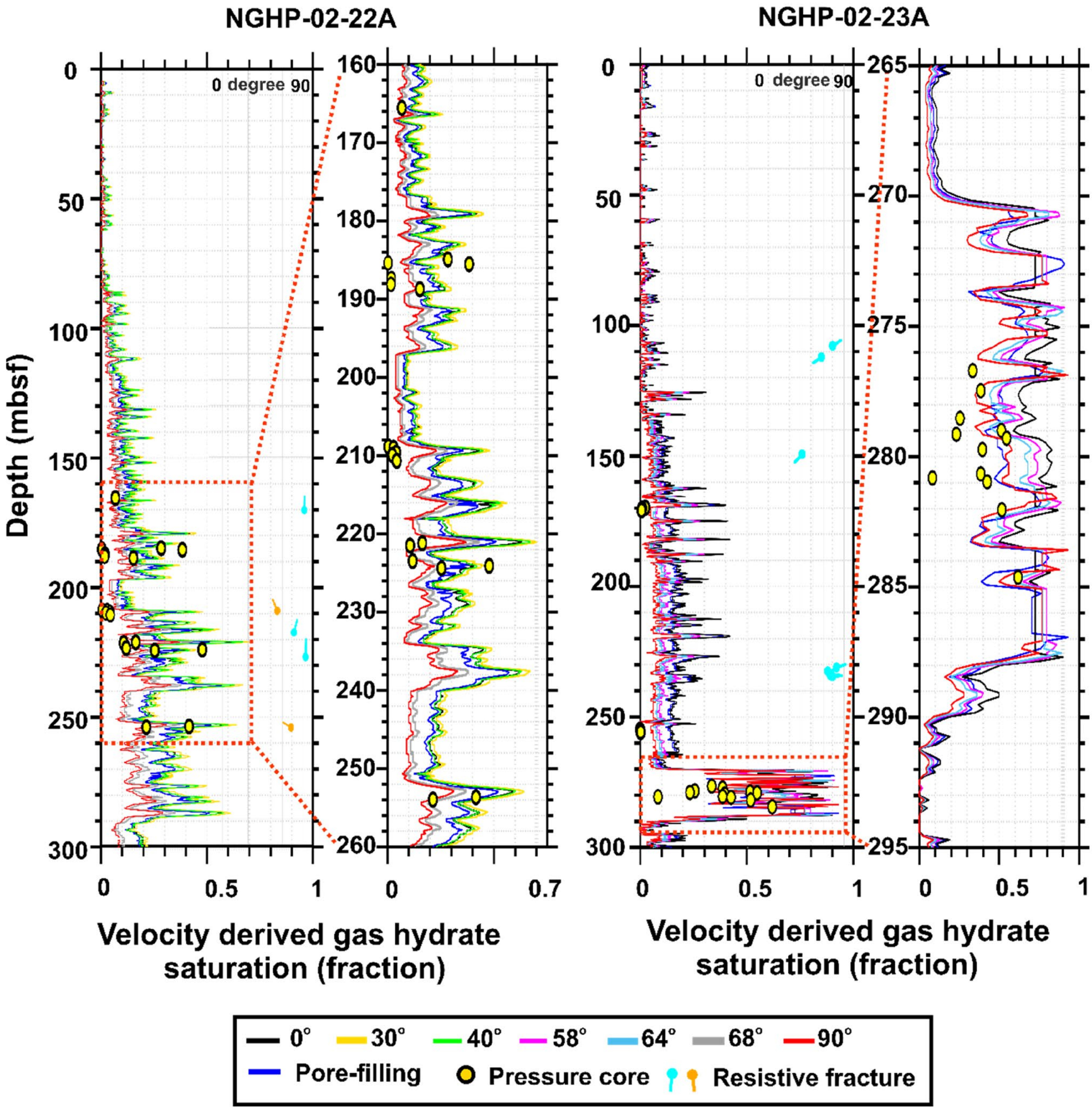

Fig. 12 Gas hydrate saturation obtained from sonic velocity and pressure cores assuming pore- and fracture-filling distributions at Hole NGHP-02-22A (left panel) and NGHP-02-23A (right panel)

RAB images and propagation resistivity curves alone are insufficient to detect fracture dips. To correctly verify the presence of the gas hydrate-filled fracture dips identified using the resistivity and velocity modelling approach, we used a combination of LWD RAB images and Propagation resistivity curves. Separation between the propagation (phase surpassing attenuation) and attenuation (phase exceeding attenuation) resistivity responses are observed when resistive gas hydrates are found in near-vertical fractures (Lee and Collett 2012). Some resistive vertical fracture dips show reverse behaviour (attenuation surpassing phase resistivity response) in the investigation, which could be attributable to the orientation of the relevant fractures. The volume fraction of gas hydrate for both pore and fracture-filling gas hydrates are calculated using confirmed fracture porosities at corresponding sites and validated with pressure core measurements from two Holes NGHP-02-22A and -02-23A. There is a good match between the resistivity-derived gas hydrate

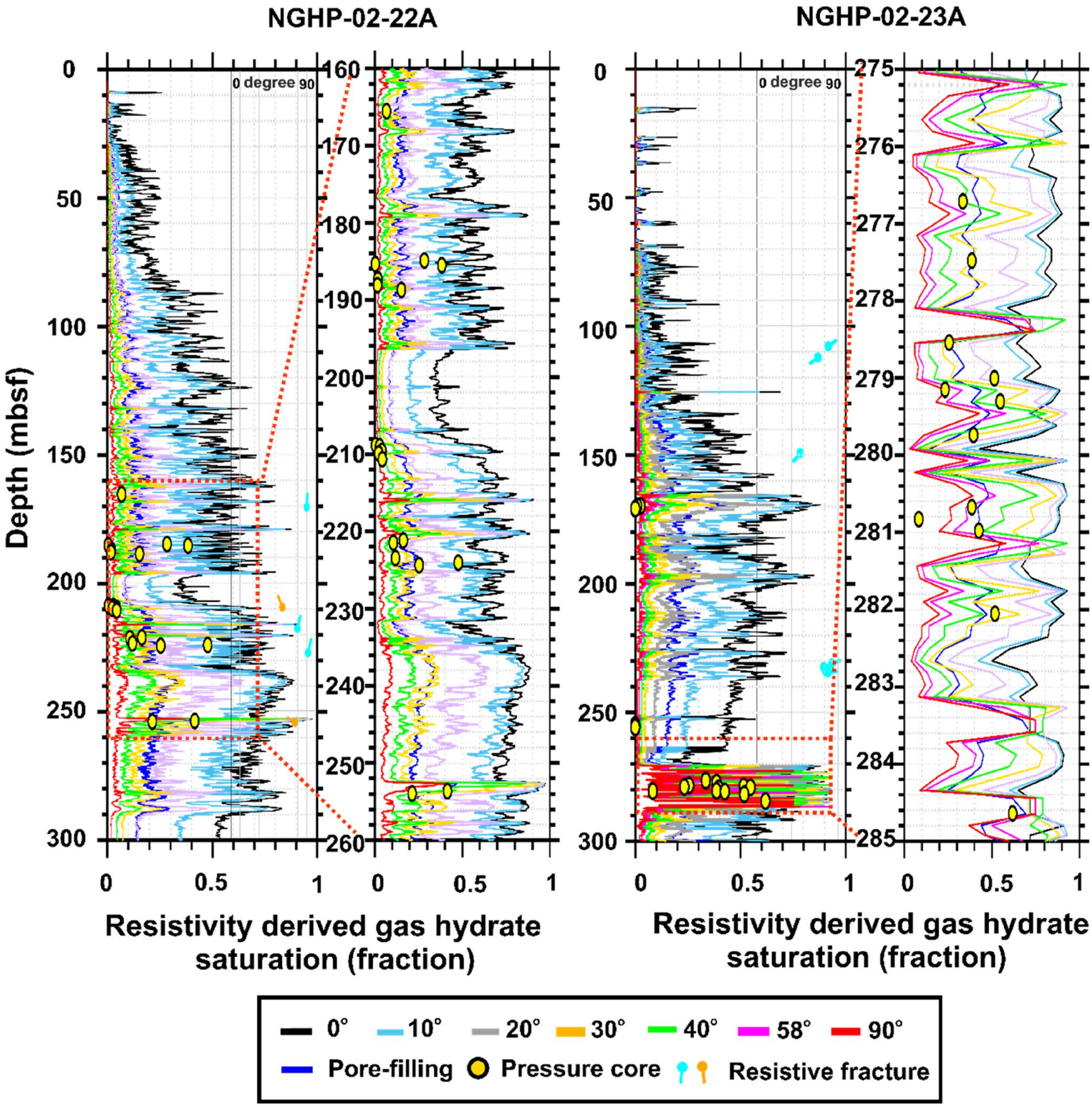

Fig. 13 Gas hydrate saturation obtained from resistivity and pressure cores assuming pore- and fracture-filling distributions at Hole NGHP-02-22A (left panel) and NGHP-02-23A (right panel)

saturations and the pressure core measurements at two holes. However, there is a significant difference between velocity-derived gas hydrate saturation estimates and pressure core data at NGHP-02-22A and -0-23A. The observed error could be: (1) due to the choice of sediment porosities, which has a significant effect on the elastic properties of the sediment, or (2) effects of the host (pore or fracture) sediments, which determine the formation and occurrence of gas hydrates, (3) due to the orientation of resistive fractures, and (4) due to the presence of higher grain density content than the grain density used in our isotropic-anisotropic based rock physics models.

Conclusions

We model the effects of borehole washouts and resistive fractures using LWD and pressure core measurements from sites NGHP-02-22 and -02-23 in the KG basin's gas hydrate-inferred Area-B. The following are the key findings of our study:

Caliper-inferred washout effects in porosity, velocity, and resistivity log measurements result in an incorrect estimation of gas hydrate saturation. The sand-shale porosity model is used to correct the porosity values.

Resistivity and velocity log measurements are corrected by assuming the washed-out column to be a seawater-filled vertical fracture, for which, we conduct a joint analysis of anisotropic resistivity and velocity responses at two sites.

The resistivity-based saturations obtained for various fracture dips match pressure core measurements at both well locations. Except for a few depths at Hole NGHP-02-22-A, the velocity-based saturations show a good match with pressure core measurements. The uncertainties associated with parameters chosen, such as sediment porosity, or assumptions made for lithology (sand and clay) content, could be plausible reasons for this mismatch.

Appendix A: Isotropic velocities

Bulk and shear modulus of the sediments using three-phase Biot-type equation (Lee and Collett 2009) are expressed as,

$$k = k_{ma}\left(1 - \beta_1\right) + \beta_1^2 K_{av}, \tag{11}$$

$$\mu = \mu_{ma}\left(1 - \beta_2\right), \tag{12}$$

where $\frac{1}{K_{av}} = \frac{(\beta_1 - \varphi)}{k_{ma}} + \frac{\varphi_w}{k_w} + \frac{\varphi_h}{k_h}$, $\beta_1 = \frac{\varphi_{as}(1+\alpha)}{(1+\alpha\varphi_{as})}$, $\beta_2 = \frac{\varphi(1+\gamma\alpha)}{(1+\gamma\alpha\varphi)}$ and $\gamma = \frac{1+2\alpha}{1+\alpha}$.

The bulk (k_{ma}) and shear modulus (μ_{ma}) of sediment matrix are calculated using Hill's average equation (Hill 1952). φ is the porosity of the sediment,$\varphi_{as} = \varphi_w + \varepsilon\varphi_h$ is the apparent porosity, $\varphi_h = S_h\varphi$ is the gas hydrate saturated porosity, $\varphi_w = \left(1 - S_h\right)\varphi$ is the water-saturated porosity and S_h is the gas hydrate saturation. The value of ε is used here as 0.12. The consolidation parameter $\alpha = \alpha_o(d_o/h)^{1/3}$, where α_o is chosen as 65 at Hole NGHP-02-22A and 45 at Hole NGHP-02-23A by calibrating the theoretical velocity of water-saturated sediment with the observed velocity of no gas hydrate zones,d_o is the maximum depth of investigation below seafloor and h is the depth below seafloor.

The P-wave velocity (V_P) for the pore-filling gas hydrate distribution is written as,

Table 1 Various constants used in rock physics modeling (Helgerud et al. 1999; Lee et al. 1996)

Bulk modulus (GPa)	Shear modulus (GPa)	Density (g/cm^3)
K_q= 38	μ_q= 44	ρ_q= 2.650
K_c= 20.9	μ_c= 6.60	ρ_c= 2.580
K_h= 8.27	μ_h= 3.49	ρ_h= 0.922
K_w= 2.29	μ_w= 0	ρ_w= 1

$$V_P = \sqrt{\frac{k + 4\mu/3}{\rho_b}}, \tag{13}$$

where $\rho_b = \rho_s(1 - \varphi) + \rho_w\varphi(1 - S_h) + \rho_h\varphi S_h$ is the bulk density of sediment, ρ_s is the matrix density, ρ_w is the density of water and ρ_h is the density of gas hydrate (see Table 1).

Acknowledgements We are thankful to the Director, CSIR-NGRI, for providing all facilities to pursue this research work and granting permission to publish this work. The Directorate General Hydrocarbons (DGH) for providing well log data and the Ministry of Earth Sciences (MoES), Delhi, are also acknowledged for research funding.

Funding This work received support from Council of Scientific and Industrial Research, India, and Ministry of Earth Sciences.

References

Archie GE (1942) The electrical resistivity log as an aid in determining some reservoir characteristics. Trans. AIME 146(01): 54–62

Arps JJ (1953) The effect of temperature on the density and electrical resistivity of sodium chloride solutions. Pet Trans. AIME 5(10): 17–20

Boswell R, Myshakin E, Moridis G, Konno Y, Collett TS, Reagan M, Ajayi T, Seol Y (2019) India national gas hydrate program expedition 02 summary of scientific results: numerical simulation of reservoir response to depressurization. Mar Pet Geol 108:154–166

Collett TS, Boswell R, Cochran JR, Kumar P, Lall M, Mazumdar A, Ramana MV, Ramprasad T, Riedel M, Sain K, Sathe AV, Vishwanath K, NGHP Expedition 01 Scientific Party (2014) Geologic implications of gas hydrates in the offshore of India: Results of the National Gas Hydrate Program Expedition 01. Marine and Petroleum Geology 58(A):3–28

Collett TS, Boswell R, Waite WF, Kumar P, Roy SK, Chopra K, Singh SK, Yamada Y, Tenma N, Pohlman J, Zyrianova M, NGHP Expedition 02 Scientific Party (2019) India National Gas Hydrate Program Expedition 02 Summary of Scientific Results: Gas hydrate systems along the eastern continental margin of India. Marine and Petroleum Geology 108:39–142

Collett TS, Riedel M, Cochran JR, Boswell R, Kumar P, Sathe AV (2008) Indian continental margin gas hydrate prospects: results of the Indian national gas hydrate program (NGHP) expedition 01, in: Proceedings of the 6th International Conference on Gas Hydrates (ICGH 2008)

Cook AE, Goldberg D (2008) Extent of gas hydrate filled fracture planes: Implications for in situ methanogenesis and resource potential. Geophys Res Lett. https://doi.org/10.1029/2008GL034587

Cook AE, Anderson BI, Malinverno A, Mrozewski S, Goldberg DS (2010) Electrical anisotropy due to gas hydrate-filled fractures. Geophysics 75:F173–F185

Dai J, Banik N, Gillespie D, Dutta N (2008) Exploration for gas hydrates in the deepwater, Northern Gulf of Mexico: Part II. Model validation by drilling. Mar Pet Geol 25(9):845–859

Dvorkin J, Nur A, Uden R, Taner T (2003) Rock physics of a gas hydrate reservoir. The Leading Edge 22(9):842–847. https://doi.org/10.1190/1.1614153

Dvorkin J, Prasad M, Sakai A, Lavoie D (1999) Elasticity of marine sediments: rock physics modeling. Geophys Res Let 26(12):1781–1784

Ecker C, Dvorkin J, Nur A (1998) Sediments with gas hydrates: internal structure from seismic AVO. Geophysics 63(5):1659–1669

Ghosh R, Ojha M (2021) Amount of gas hydrate estimated from rock physics analysis based on morphology and intrinsic anisotropy in area B, Krishna Godavari offshore basin, expedition NGHP-02. Mar Pet Geol 124:104856

Ghosh R, Sain K, Ojha M (2010) Effective medium modeling of gas hydrate-filled fractures using the sonic log in the Krishna-Godavari basin, offshore eastern India. J Geophys Res Solid Earth. https://doi.org/10.1029/2009JB006711

Helgerud MB, Dvorkin J, Nur A, Sakai A, Collett T (1999) Elastic-wave velocity in marine sediments with gas hydrates: effective medium modeling. Geophys Res Lett 26(13):2021–2024

Hill R (1952) The elastic behaviour of a crystalline aggregate. Proc Phys Soc Am 65:349

Huang T, Zhang Y, Li G, Li X, Chen Z (2020) Numerical modeling for drilling fluid invasion into hydrate-bearing sediments and effects of permeability. J Nat Gas Sci Eng 77:103239

Jakobsen M, Hudson JA, Minshull TA, Singh SC (2000) Elastic properties of hydrate-bearing sediments using effective medium theory. J Geophys Res Solid Earth 105(B1):561–577

Jana S, Ojha M, Sain K (2015) Gas hydrate saturation from heterogeneous model constructed from well log in Krishna-Godavari Basin, Eastern Indian Offshore. Geophys J Int 203:184–194

Jana S, Ojha M, Sain K, Srivastava S (2017) An approach to estimate gas hydrate saturation from 3-D heterogeneous resistivity model: a study from Krishna-Godavari basin, Eastern Indian offshore. Mar Pet Geol 79:99–107

Joshi AK, Sain K, Pandey L (2019) Gas hydrate saturation and reservoir characterization at sites NGHP-02-17 and NGHP-02-19, Krishna Godavari Basin, eastern margin of India. Mar Pet Geol 108:595–608

Kennedy WD, Herrick DC (2004) Conductivity anisotropy in shale-free sandstone. Petrophysics 45:SPWLA-2004-v45n1a3

Koltermann CE, Gorelick SM (1995) Fractional packing model for hydraulic conductivity derived from sediment mixtures. Water Resources Research 31(12):3283–3297. https://doi.org/10.1029/95WR02020

Kvenvolden KA (1988) Methane hydrate—a major reservoir of carbon in the shallow geosphere. Chem Geol 71:41–51

Lee MW (2012) Isotropic, anisotropic, and borehole washout analyses in Gulf of Mexico Gas Hydrate Joint Industry Project Leg II, Alaminos Canyon well 21-A. US Geol Surv Sci Invest Rep 5046:23

Lee MW, Collett TS (2009) Gas hydrate saturations estimated from fractured reservoir at Site NGHP-01-10, Krishna-Godavari Basin, India. J Geophys Res Solid Earth. https://doi.org/10.1029/2008JB006237

Lee MW, Collett TS (2012) Pore-and fracture-filling gas hydrate reservoirs in the Gulf of Mexico gas hydrate joint industry project leg II Green Canyon 955 H well. Mar Pet Geol 34:62–71

Lee MW, Collett TS, Lewis KA (2012) Anisotropic models to account for large borehole washouts to estimate gas hydrate saturations in the Gulf of Mexico Gas Hydrate Joint Industry Project Leg II Alaminos Canyon 21 B well. Mar Pet Geol 34(1):85–95

Lee MW, Hutchinson DR, Collett TS, Dillon WP (1996) Seismic velocities for hydrate-bearing sediments using weighted equation. J Geophys Res Solid Earth 101:20347–20358

Liu T, Liu X, Zhu T (2020) Joint analysis of P-wave velocity and resistivity for morphology identification and quantification of gas hydrate. Mar Pet Geol 112:104036

Makogon YF (2010) Natural gas hydrates—a promising source of energy. J Nat Gas Sci Eng 2(1):49–59

Marion D, Nur A, Yin H, Han DH (1992) Compressional velocity and porosity in sand-clay mixtures. Geophysics 57:554–563

Ojha M, Ghosh R (2021) Assessment of gas hydrate using prestack seismic inversion in the Mahanadi Basin, offshore eastern India. Interpretation 9(2):SD15–SD26

Ojha M, Sain K (2013) Quantification of gas hydrate and free gas in the Andaman offshore from downhole data. Curr Sci 105:512–516

Ojha M, Sen MK, Sain K (2016) Use of split spread configuration of marine multichannel seismic data in full waveform inversion, Krishna-Godavari basin. India J Seism Explor 25(4):359–373

Pandey L, Sain K, Joshi AK (2019) Estimate of gas hydrate saturations in the Krishna-Godavari basin, eastern continental margin of India, results of expedition NGHP-02. Mar Pet Geol 108:581–594

Phillips SC, Johnson JE, Underwood MB, Guo J, Giosan L, Rose K (2014) Long-timescale variation in bulk and clay mineral composition of Indian continental margin sediments in the Bay of Bengal, Arabian Sea, and Andaman Sea. Mar Pet Geol 58:117–138

Pratson LF, Stroujkova A, Herrick D, Boadu F, Malin P (2003) Predicting seismic velocity and other rock properties from clay content only. Geophysics 68(6):1847–1856

Ruppel CD, Kessler JD (2017) The interaction of climate change and methane hydrates. Rev Geophysics 55:126–168

Sain K, Ojha M (2008) Identification and quantification of gas hydrates: a viable source of energy in the 21st century. Mem Geol Soc India 68:273–288

Singh A, Ojha M, Sain K (2020) Predicting lithology using neural networks from downhole data of a gas hydrate reservoir in the Krishna-Godavari basin, eastern Indian offshore. Geophys J Int 220(3):1813–1837

Sloan ED Jr, Koh CA (2007) Clathrate hydrates of natural gases. CRC Press, Florida

Tinivella U (1999) A method for estimating gas hydrate and free gas concentrations in marine sediments. Bollettino Di Geofisica Teorica Ed Applicata 40(1):19–30

Waite WF, Ruppel CD, Collett TS, Schultheiss P, Holland M, Shukla KM, Kumar P (2019) Multi-measurement approach for establishing the base of gas hydrate occurrence in the Krishna-Godavari Basin for sites cored during expedition NGHP-02 in the offshore of India. Mar Pet Geol 108:296–320

Wang X, Sain K, Satyavani N, Wang J, Ojha M, Wu S (2013) Gas hydrates saturation using geostatistical inversion in a fractured reservoir in the Krishna-Godavari basin, offshore eastern India. Mar Pet Geol 45:224–235

Wang Y, Yang Y, Wang K, Tao L, Liu J, Wang C, Yao J, Zhang K, Song W (2020) Changes in relative permeability curves for natural gas hydrate decomposition due to particle migration. J Nat Gas Sci Eng 84:103634

White JE (1965) Seismic waves: radiation, transmission, and attenuation. McGraw-Hill, New York

Yadav US, Shukla KM, Ojha M, Kumar P, Shankar U (2019) Assessment of gas hydrate accumulations using velocities derived from vertical seismic profiles and acoustic log data in Krishna-Godavari Basin, India. Mar Pet Geol 108:551–561

Publisher's Note Springer Nature remains neutral with regard to jurisdictional claims in published maps and institutional affiliations.

Springer Nature or its licensor holds exclusive rights to this article under a publishing agreement with the author(s) or other rightsholder(s); author self-archiving of the accepted manuscript version of this article is solely governed by the terms of such publishing agreement and applicable law.